

Ring-exchange periodic Anderson model for ^3He bilayers

Jan Werner* and Fakher F. Assaad

*Institut für Theoretische Physik und Astrophysik,
Universität Würzburg, Am Hubland, 97074 Würzburg, Germany*

(Dated: June 7, 2021)

We present numerical results of a model calculation for the ^3He bilayer system, which captures the interplay between fast and slow dynamics of the different layers and incorporates an independent scale for the three body ring exchange. By means of cluster dynamical mean-field theory in conjunction with continuous-time quantum Monte Carlo, we find remarkable similarities with the experiments: a suppression of the coherence temperature upon approaching the solidification point of the first layer accompanied by the onset of strong ferromagnetic correlations within the first layer. Based on the consistent results for different cluster sizes we conjecture a first-order transition cutting short the Kondo breakdown, which allows us to interpret the experimental observation of an intervening phase preempting the quantum critical point in terms of a phase separation.

PACS numbers: 71.10.-w, 71.27.+a, 75.30.Mb

I. INTRODUCTION

Heavy fermion systems remain a subject of strong interest, even after decades of intense research activity^{1,2}. Heavy fermion superconductivity³, quantum criticality, the competition and coexistence of Fermi-liquid coherence and magnetic order⁴⁻¹⁰, and the recent proposal of a topologically non-trivial ground state in heavy fermion compounds^{11,12} stand as important topics.

^3He represents a unique realization of a Fermi liquid^{13,14}. In particular, layered systems of ^3He have been used in different experiments to realize unique Fermi-liquid ground states. What makes this system especially interesting is that the relative strength of the interaction and kinetic energy can be varied by choosing suitable substrates, and by tuning the filling. In heat capacity measurements on ^3He monolayers on graphite, a linear dependence on temperature characteristic of a Fermi liquid was observed¹⁵. By tuning the filling, the linear coefficient γ can be varied, and it even diverges at a critical filling, which marks the solidification of the monolayer. This provides a realization of a filling controlled Mott metal-insulator transition in two dimensions which is driven by the divergence of the effective mass¹⁶. In another setup with ^3He on a substrate of four layers of ^4He , with two being solid and two superfluid, on top of graphite, a series of steps as a function of filling were observed in the γ coefficient¹⁷. This was attributed to the population of additional, excited states, which results in enhanced quasiparticle interactions.

The results of experiments conducted on a bilayer system of ^3He have been interpreted in terms of heavy fermion physics¹⁸. What makes this particular setup so interesting is that the first layer remains fluid as the second layer is forming, and it only solidifies at a somewhat larger filling. It is the interplay between the slow dynamics of the strongly correlated first-layer fermions, which are close to solidification, and the fast dynamics of the weakly correlated second-layer fermions, which drives the heavy fermion physics in this particular sys-

tem. Hence, a heavy fermion phase is observed, where due to the Kondo effect, fermions of the different layers form coherent quasiparticles of composite character. Accordingly, the magnetic moment of the nearly localized first-layer fermions is screened by the delocalized second-layer fermions, resulting in a Pauli magnetic susceptibility. The coherence temperature T_{coh} as the characteristic low energy scale corresponds to a large mass renormalization.

These experiments clearly show that the bilayer of ^3He is a unique realization of heavy fermion physics. The specific heat below T_{coh} depends linearly on temperature, while the magnetization curve saturates to a constant. With increasing filling the coherence scale T_{coh} is suppressed due to the density-dependent effective hybridization. By extrapolation, T_{coh} is found to vanish at a critical filling n_C where the effective mass diverges; the Kondo effect breaks down at a quantum critical point (QCP) and the first layer solidifies. This orbital-selective Mott transition makes the first layer a local moment ferromagnet, while the second layer is a fluid overlayer. However, in the experiments quantum criticality is preempted by an intervening phase at filling $\langle n \rangle_I < \langle n \rangle_C$, identified by the onset of a finite magnetization at the lowest temperature. This indicates that the magnetic exchange coupling, which results from three particle ring exchange processes¹⁹⁻²¹, is becoming the dominant energy scale, and leads to strong ferromagnetic fluctuations.

The aim of this paper is to introduce a model which captures the minimal ingredients of the ^3He bilayer: Kondo screening, the hard core character of the ^3He atoms as well as the three particle ring exchange which triggers ferromagnetic fluctuations in the first layer. In Sec. II we will introduce the model, and show how to solve it within cluster dynamical mean-field theory (DMFT). Since we are dealing with a strong coupling problem, we will use the continuous time hybridization expansion quantum Monte Carlo algorithm^{22,23} as a cluster solver.

In Secs. III and IV we detail our numerical results for

various cluster sizes. A comparison with the experimental data of Ref. 18 as well as an interpretation of our results is provided in the discussion and conclusion Sec. V.

II. MODEL AND METHOD

In a series of studies, model Hamiltonians based on the bilayer Hubbard model and periodic Anderson model have been put forward to understand the physics of the ^3He bilayers. In Refs. 24, 25 and 26 a slave boson approximation which captures the Fermi-liquid ground state but neglects local moment formation was used. There, a vanishing of the effective hybridization was found to occur prior to the QCP inferred from extrapolating the coherence scale.

A cluster DMFT study of the bilayer Hubbard model was presented in Refs. 27 and 28. However, the numerical investigation was plagued by an odd-even effect, where competing ground states are realized, which are favored by clusters with an odd and even number of sites, respectively. In the current study, we bring forward a similar model, but with some very important differences. We start with the same two-band Hubbard model, with the two layers arranged in a close-packed triangular lattice as schematically shown in Fig. 1. In contrast to the previous works, we incorporate an independent scale for the three body ring exchange as well as the constraint of no double occupancy. This leads to the Hamiltonian

$$\begin{aligned} \hat{H} &= \hat{H}_0 + \hat{H}_I \quad (1) \\ \hat{H}_0 &= \sum_{k,\sigma} \begin{pmatrix} c_{k,\sigma}^\dagger & f_{k,\sigma}^\dagger \end{pmatrix} \begin{pmatrix} \varepsilon_C(k) & V(k) \\ V(k)^* & \varepsilon_f(k) \end{pmatrix} \begin{pmatrix} c_{k,\sigma} \\ f_{k,\sigma} \end{pmatrix} \\ \hat{H}_I &= \lim_{U \rightarrow \infty} \frac{U}{2} \sum_i n_{f,i} (n_{f,i} - 1) - J \sum_{\langle i,j \rangle} S_{f,i} S_{f,j} \end{aligned}$$

where we label first-layer fermions as $f_{k,\sigma}$ and second-layer fermions as $c_{k,\sigma}$, with momentum k and spin σ . As a result of interlayer and intralayer hopping we obtain the dispersions $\varepsilon_c(k)$ and $\varepsilon_f(k)$ and a momentum dependent hybridization $V(k)$:

$$\begin{aligned} \varepsilon_c(k) &= -2t_c \gamma(k) \quad (2) \\ \varepsilon_f(k) &= E_f - 2t_f \gamma(k) \\ V(k) &= V_{cf} \sqrt{3 + 2\gamma(k)} \\ \gamma(k) &= \cos(k \cdot a_1) + \cos(k \cdot a_2) + \cos(k \cdot (a_1 - a_2)). \end{aligned}$$

E_f is an energy offset which models the difference in binding energies of the first and second layer. The hardcore constraint of the ^3He atoms is taken into account by the limit $U \rightarrow \infty$, which allows us to project out all states with double occupancy. The three body ring exchange gives rise to an effective ferromagnetic coupling between nearest-neighbor spins²⁰. Hence, to explicitly include the

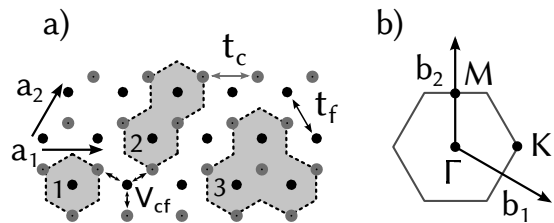


FIG. 1. a) Real-space arrangement of ^3He atoms in the bilayer system. $a_{1,2}$ are the lattice unit vectors. Second-layer sites (gray) are on top of and shifted with respect to sites in the first layer (black). The double arrows indicate intralayer hopping with amplitude $t_{c,f}$ and interlayer hopping, i.e. hybridization with amplitude V_{cf} . The shaded areas represent the cluster geometries employed, containing respectively one (1), two (2) and three (3) correlated first-layer sites. b) First Brillouin zone of the triangular lattice, with reciprocal lattice vectors $b_{1,2}$ and high-symmetry points.

ring exchange, we introduce a Heisenberg spin-spin exchange interaction between neighboring sites $\langle i, j \rangle$, with a ferromagnetic coupling constant $J > 0$.

Note that we neglect the effect of correlations in the second layer, which is justified as long the filling of this layer is significantly smaller than 1, i.e. half-filling, such that correlations result at most in a mild renormalization of the band dispersion.

Our model hence contains relevant magnetic interactions for ^3He . In particular, since $U \rightarrow \infty$, superexchange is blocked. On the other hand the Ruderman-Kittel-Kasuya-Yoshida (RKKY) interaction will be dynamically generated and will compete with the ring exchange.

The concrete parameter values we choose are $t_f = t_c = t$, $V_0/t = 0.5$, $J/t = 0.3$ and $E_f/t = -4.0$. We study the model in the grandcanonical ensemble as a function of the chemical potential μ , which the density couples to, and the inverse temperature $\beta = 1/T$.

To make this model accessible to numerical simulations, we use the cellular DMFT²⁹, which is a real-space cluster extension to the dynamical mean-field theory³⁰, and hence yields results in the thermodynamic limit. In this scheme the lattice self-energy is approximated to be independent of momentum in the reduced Brillouin zone of the super cell, while it retains its dependence on frequency. This approximate self-energy is obtained from an effective cluster of N_c correlated sites embedded in a non-interacting bath described by the hybridization function $\Delta(i\omega)$. This quantity connects the auxiliary cluster problem with the original lattice problem via the self-consistency condition

$$\mathbf{G}_{imp}(i\omega) = \frac{N_c}{N} \sum_{\tilde{k}} \mathbf{G}_{latt}(\tilde{k}, i\omega) \quad (3)$$

between the impurity Green's function \mathbf{G}_{imp} and the lo-

cal lattice Green's function

$$\mathbf{G}_{imp}(i\omega)^{-1} = i\omega \mathbf{m} - \mathbf{t}_f - \mathbf{\Delta}(i\omega) - \mathbf{\Sigma}(i\omega) \quad (4)$$

$$\left[\mathbf{G}_{latt}(\tilde{k}, i\omega) \right]_{ij} = \frac{1}{N_c} \sum_K \mathbf{G}_{latt}(\tilde{k} + K, i\omega) e^{iK \cdot (R_i - R_j)}.$$

All quantities are matrices in cluster space and, in principle, depend on spin. As we will limit ourselves to the paramagnetic, symmetry-unbroken state, we neglect the spin index. \tilde{k} is a momentum in the reduced Brillouin zone, while R and K are the positions of the cluster sites in real space and reciprocal space, respectively. This method takes dynamical fluctuations fully into account, thus capturing the physics of Kondo screening, but it also incorporates non-local correlations to describe the magnetic exchange. It is thus very well suited to study models with local and short-ranged correlations³¹. It is precisely the competition between these two interactions which determines the behavior of the system, and which is at the heart of heavy fermion physics. The relatively large coordination number ($Z = 6$) of the lattice at hand means that the approximation of cluster DMFT can yield reasonable results.

To obtain the self-energy $\mathbf{\Sigma}(i\omega)$ within each step of the self-consistency loop, we solve the effective cluster problem by means of continuous time hybridization expansion quantum Monte Carlo^{22,23}. This numerically exact method systematically samples diagrams from the series expansion of the partition function Z corresponding to the effective action S_{eff} ,

$$S_{eff} = S_c + \int_0^\beta d\tau d\tau' \sum f^\dagger(\tau) \mathbf{\Delta}(\tau - \tau') f(\tau') \quad (5)$$

$$\frac{Z}{Z_{loc}} = \sum_{n=0}^{+\infty} \sum_{\{\alpha, \alpha'\}} \frac{1}{n!} \int_0^\beta d\tau_1 d\tau'_1 \cdots d\tau_n d\tau'_n \quad (6)$$

$$\times \langle T_\tau f_{\alpha_1}^\dagger(\tau_1) f_{\alpha'_1}(\tau'_1) \cdots f_{\alpha_n}^\dagger(\tau_n) f_{\alpha'_n}(\tau'_n) \rangle_{loc}$$

$$\times \frac{1}{n!} \det [\Delta_{\alpha_i \alpha_j}(\tau_i - \tau'_j)].$$

S_c denotes the contribution of the local impurity, and we used the shorthand notation $f = (f_\alpha) = (f_{1,\uparrow}, f_{1,\downarrow}, \dots, f_{N_c,\uparrow}, f_{N_c,\downarrow})$. The operator expectation value $\langle \cdots \rangle_{loc}$ is taken with respect to the cluster part of the Hamiltonian.

This method is very efficient in the regime of strong interactions, and is able to treat arbitrary local (restricted to the cluster) interactions such as Hund's rule coupling or ring exchange. The drawback is that the numerical effort scales exponentially with the number of cluster sites or orbitals³². In principle, by exploiting symmetries, such as the total particle number N , the z -component of the total spin S_z ²³, and the projected singlet quantum number³³, and thereby splitting the matrices into blocks, one can reduce the computational complexity. However, in our case, due to the hopping between cluster sites, this approach is limited to N and S_z .

In addition, while absent for single-site calculations, in effective cluster simulations for cluster DMFT there is a sign problem, which prohibits us from simulating clusters with more than three correlated f -sites at sufficiently low temperatures.

However, since the effective nearest-neighbor magnetic exchange is explicitly included in the Hamiltonian (1), even small clusters already include important aspects of the ring exchange physics. Therefore, even a cluster of size $N_c = 2$ represents a significant improvement over single-site DMFT, where ring exchange is completely neglected.

In the following we present our results with plots for $N_c = 2$ and $N_c = 3$ side-by-side, where appropriate. However, to make the discussion of the results more coherent, in the text we focus on the case $N_c = 3$.

III. FERMI LIQUID REGIME

Starting at less than half filling of the first layer, the hybridization with the delocalized second-layer fermions leads to a crossover from an incoherent regime at high temperatures to a regime of coherent heavy quasiparticles, which takes place at a characteristic scale, the coherence temperature T_{coh} . This crossover can be seen in the inverse of the transverse static susceptibility of the f -spins,

$$\chi_f = \chi_f(i\nu = 0) = \frac{1}{V} \left. \frac{dM_f}{dB} \right|_{B=0}. \quad (7)$$

Here we have approximated the lattice susceptibility by the cluster susceptibility,

$$\chi_f(i\nu) \approx \chi_f^{(C)}(i\nu) = \frac{1}{N_c} \sum_{i,j=1}^{N_c} \int_0^\beta d\tau \langle S_i^z(\tau) S_j^z(0) \rangle. \quad (8)$$

The static susceptibility is shown in Fig. 2. At high temperatures, the susceptibility follows a Curie-Weiss law $\chi_f \sim \frac{1}{T-\theta}$, which is the expected behavior for local moments. The ferromagnetic coupling J leads to an increase in the susceptibility compared to the case of isolated moments ($\theta = 0$), and thus gives rise to a finite Weiss temperature $\theta > 0$. For $\mu/t \leq -0.77$, the susceptibility clearly deviates from the Curie-Weiss behavior at the lowest temperatures. Instead χ_f extrapolates to a finite value as $T \rightarrow 0$. This corresponds to a complete screening of the f -moments by the Kondo effect due to spin-flip scattering of the c -fermions off the f -moments, and it is precisely the Pauli paramagnetism expected for a Fermi liquid. Due to a severe negative sign problem, for $\mu/t \leq -0.80$ we are restricted to inverse temperatures $\beta t \leq 40$. However, this is below T_{coh} , so that the crossover to the Fermi-liquid state can be nicely resolved. For $\mu/t \geq -0.75$, the situation seems to change rather abruptly. χ_f approaches the Curie-law behavior at the

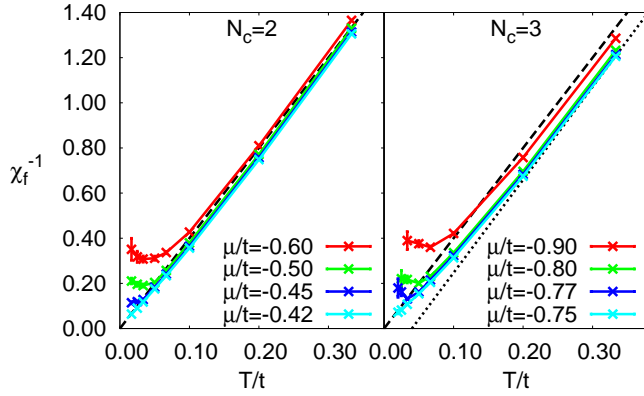


FIG. 2. Transverse static f -spin susceptibility obtained from the cluster. In the local-moment regime, the layers are uncoupled, with a behavior according to a Curie-Weiss law, while below T_{coh} the f -spins are screened and exhibit a Pauli susceptibility. The black dashed line is the Curie susceptibility ($\theta = 0$), while the dotted line corresponds to $\theta = 0.04t$.

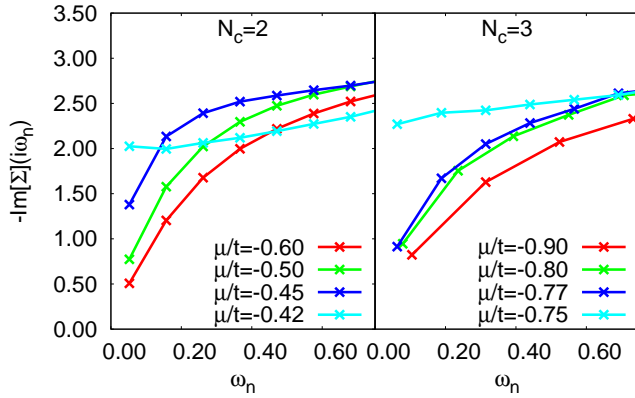


FIG. 3. Imaginary part of the local self-energy for the clusters of size $N_c = 2$ and $N_c = 3$, and at the lowest temperatures attainable. For $\mu/t \leq -0.45$ ($\mu/t \leq -0.77$), it is linear at small frequencies, which signifies the existence of a Fermi liquid at low temperatures.

lowest temperature attainable; that is the local moments are not screened.

On the real frequency axis and for the generic Fermi-liquid state, the low frequency behavior of the self-energy is characterized by $\text{Im}[\Sigma(\omega)] \sim \omega^2$, and $\text{Re}[\Sigma(\omega)] \sim a + b\omega$. For Matsubara frequencies, this implies that $\text{Im}[\Sigma(i\omega_m)] \sim \omega_m$. In Fig. 3 the low-frequency imaginary part of the local self-energy is plotted. For smaller values of μ/t there is a clear signature of a Fermi-liquid ground state. Beyond a certain threshold value, an extrapolation to zero with $\omega \rightarrow 0$ is clearly not possible.

The linear coefficient of the self-energy at small frequencies is related to the coherence temperature T_{coh} , quasiparticle residue Z , and effective mass ratio m^*/m

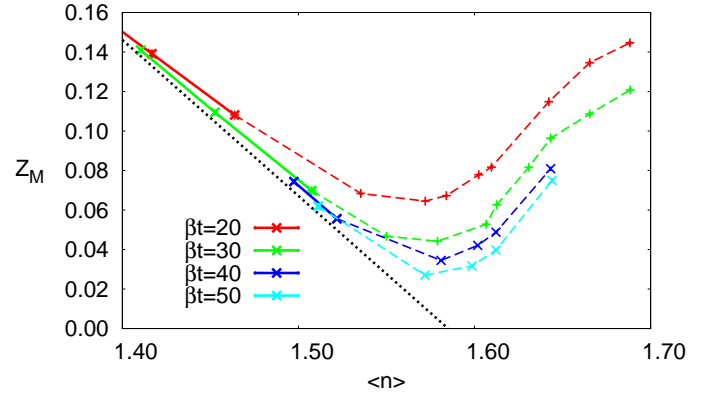


FIG. 4. Quasi-particle residue Z approximated by Z_M as defined in (10) for different temperatures, derived from the results for $N_c = 3$. The dashed lines imply that either the imaginary part of the self-energy is not yet linear in frequency because of the high temperature or Z is not well defined because the self-energy is not linear at all above the critical filling. The dotted line is a guide to the eye to show the apparent vanishing of Z at a QCP.

via

$$T_{\text{coh}}^{-1} \sim Z^{-1} = \frac{m^*}{m} = 1 - \left. \frac{d\Sigma(\omega)}{d\omega} \right|_{\omega=0}, \quad (9)$$

which we approximate using the first Matsubara frequency value via

$$Z^{-1} \approx Z_M^{-1} = 1 - \frac{\text{Im}[\Sigma(i\pi T)]}{\pi T}. \quad (10)$$

Within the Fermi-liquid regime, the onset of coherence shifts to lower temperatures with increasing chemical potential. This gradual suppression of the coherence scale and quasiparticle residue, or equivalently the increase of the quasiparticle effective mass, results from the renormalization of the effective hybridization due to the increasing filling. The evolution of Z_M , i.e. the inverse effective mass, is shown in Fig. 4 versus the total filling $\langle n \rangle = \langle n_f + n_c \rangle$. At $n \leq 1.5$ the results for Z_M converge at low temperatures, $Z_M(T \rightarrow 0) \rightarrow Z$, once the coherent Fermi-liquid state is established. As a function of filling, the quasiparticle residue changes approximately linearly. With increasing μ , Z is increasingly suppressed and by extrapolation seems to vanish at a critical filling $\langle n \rangle_C \approx 1.58$ at a QCP.

IV. MAGNETIC CROSSOVER

While increasing μ , the behavior of the observables considered above changes abruptly at a certain threshold value of μ , with clear deviations from the Fermi-liquid results. To learn more about what happens there, we show in Fig. 5 the evolution of the f -orbital occupation as a function of chemical potential μ/t and inverse temperature βt . With decreasing temperature a rather strong

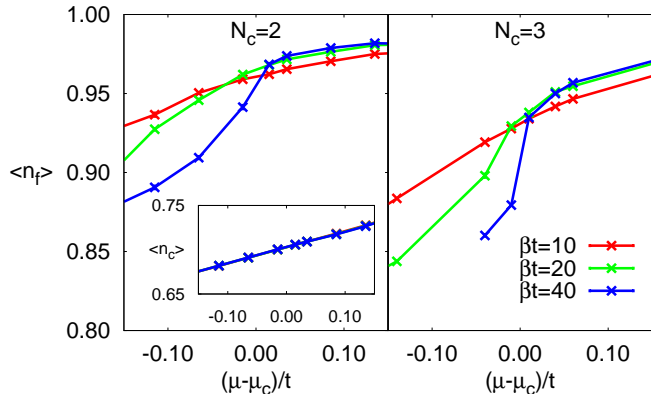


FIG. 5. f -orbital occupation number for both cluster geometries. At lower temperature, the occupation exhibits a strong increase upon crossing μ_C , which is even steeper for the larger cluster. The f -filling exhibits a strong temperature dependence for $\mu < \mu_C$, but is only weakly temperature dependent beyond μ_C . The inset shows the filling of the second layer for $N_c = 2$, which is much smaller than 1. Thus, neglecting correlations for the c -fermions is well-justified. In contrast to $\langle n_f \rangle$, the c -filling has almost no temperature dependence.

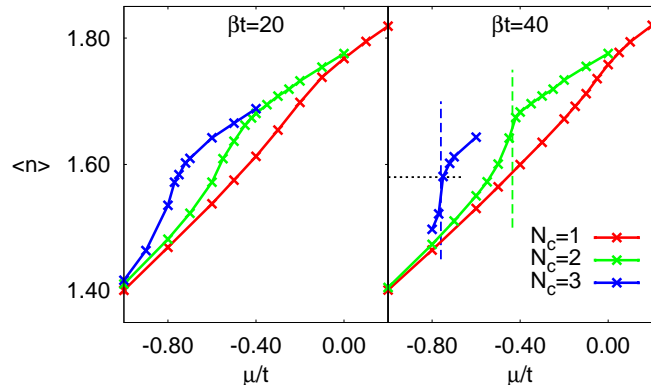


FIG. 6. Total occupation number for $N_c = 1 - 3$, at two inverse temperatures βt . The dashed lines indicate the location of μ_C for $N_c = 2$ and 3, while the black dotted line is the critical filling $\langle n \rangle_C \approx 1.58$ obtained for $N_c = 3$.

increase of the f -orbital occupation develops in a very narrow window of μ -values. We define a characteristic value of the chemical potential μ_C by the largest step between subsequent values of μ .

In addition, we compare in Fig. 6 the total particle number for all cluster sizes at two different temperatures. Looking at the trend from $N_c = 1 - 3$, the increase around μ_C becomes steeper for larger clusters and lower temperatures, but stays continuous. It is interesting to note that the putative QCP at filling $\langle n \rangle_C$ seems to be located more or less inside the step in occupation.

Next, we look at the nearest-neighbor spin-spin corre-

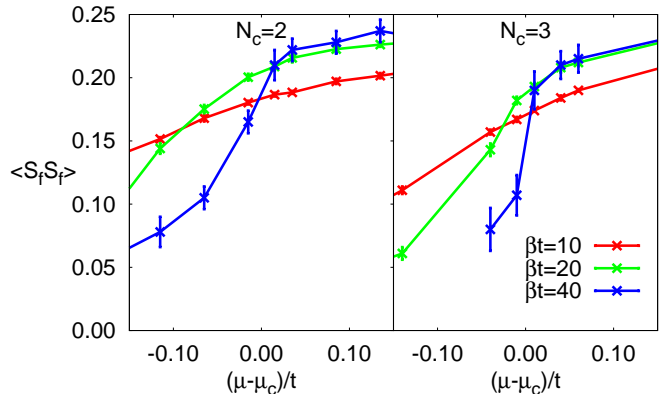


FIG. 7. Spin-spin correlation between neighboring f -sites, obtained from the cluster. While there is little correlation in the incoherent and heavy fermion phase, beyond μ_C the spins are almost fully polarized.

lation between f -orbitals,

$$\langle S_f S_f \rangle = \frac{1}{N_p} \sum_{\langle i, j \rangle} \langle S_{f,i} S_{f,j} \rangle, \quad (11)$$

normalized by the number of distinct pairs $\langle i, j \rangle$ of neighboring sites N_p , which is shown in Fig. 7. For smaller filling, the observed correlation extrapolates to a small value as $T \rightarrow 0$. This is consistent with the interpretation of a Fermi-liquid state, where the moments are predominantly screened by the second-layer light fermions. Beyond the point $\mu = \mu_C$, we observe a completely different behavior: a large correlation which seems to grow and eventually saturate at lower temperatures. Apparently, for $\mu > \mu_C$ there are strong ferromagnetic fluctuations; that is, a parallel alignment of neighboring f -spins is favored.

Finally, we show in Fig. 8 the momentum-resolved spectral function obtained by analytical continuation of the Green's function from Matsubara frequencies to real frequencies³⁴, which we obtain from the periodized f -orbital self-energy $\Sigma(k, i\omega)$

$$A(k, \omega) = -\pi^{-1} \text{Im}[\text{Tr} \mathbf{G}(k, \omega)] \quad (12)$$

$$\mathbf{G}(k, i\omega) = \begin{pmatrix} i\omega + \mu - \varepsilon_c(k) & -V(k) \\ -V(k)^* & i\omega + \mu - \varepsilon_f(k) - \Sigma(k, i\omega) \end{pmatrix}^{-1}$$

In the two left panels in Fig. 8, where $\mu < \mu_C$, the hybridization between the two bands is clearly visible, which leads to the heavy-fermion band close to the Fermi level, and a small gap at the points of avoided crossing. With the suppression of the coherence scale, the heavy band becomes even flatter. At $\mu > \mu_C$, the hybridization is almost completely gone. The c -band goes straight through the points, where previously a crossing was avoided by the hybridization. The spectral weight from the heavy-fermion band is largely gone, because it is transferred to the broad, incoherent features far below the Fermi level.

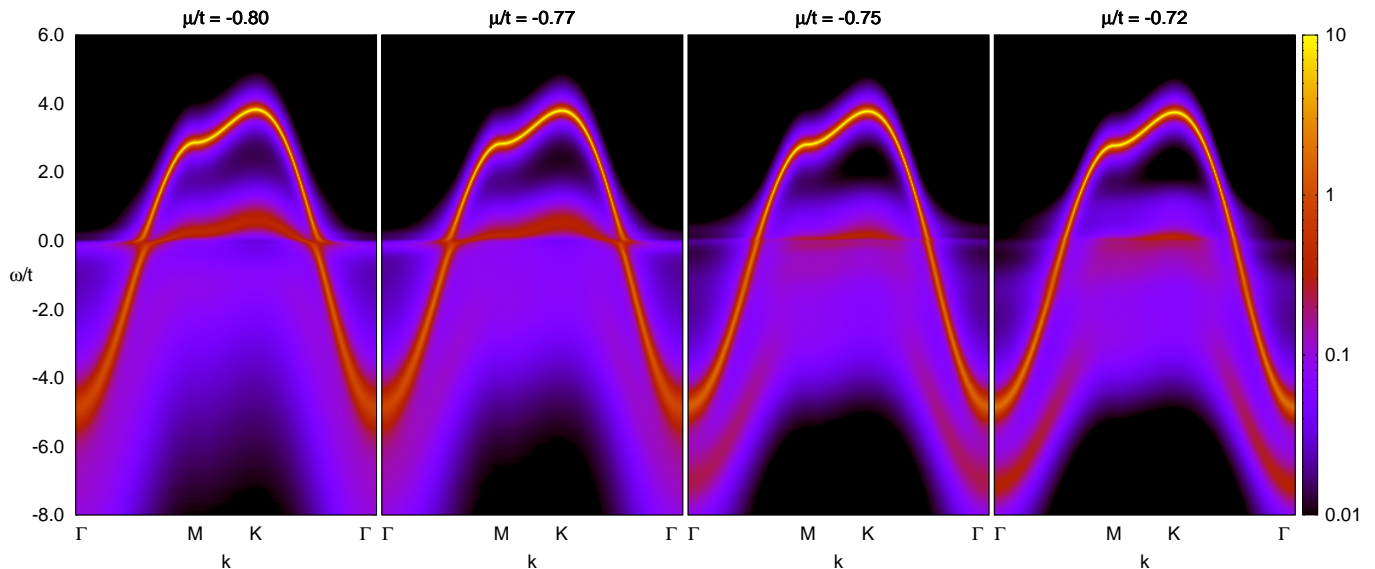


FIG. 8. Spectral function $A(k, \omega)$ for $N_c = 3$, at inverse temperature $\beta t = 40$. For $\mu/t \leq -0.77$ the heavy-fermion bands are clearly visible, while for larger μ there is little spectral weight left at the Fermi energy.

V. DISCUSSION AND CONCLUSIONS

Our model captures nicely the Fermi-liquid regime, where we recover the crossover from the incoherent regime to the Fermi-liquid state of strongly renormalized quasiparticles. The coherence temperature T_{coh} , which marks the onset of Fermi-liquid behavior, is suppressed by increasing the filling $\langle n \rangle$. Extrapolating T_{coh} for fillings $\langle n \rangle < 1.5$, where results are converged in temperature, defines a quantum critical point at $\langle n \rangle_C = 1.58$ where T_{coh} vanishes and the Kondo effect breaks down.

As the coherence temperature drops, or, equivalently, the effective mass grows, the model system becomes increasingly susceptible to ferromagnetic fluctuations triggered by the three site ring exchange term which competes with Kondo screening. Indeed, our numerical results show a crossover to a state with robust ferromagnetic correlations within the first layer. This is accompanied by a strong increase in the occupation of the first layer. At the same time, the high temperature spin susceptibility shows a Curie-Weiss law with a robust positive Weiss constant, which is appropriate for a ferromagnetic transition. At low temperatures, and on our finite size clusters, the Curie-Weiss law gives way to a finite a Pauli spin susceptibility. This low temperature behavior is clearly very sensitive to the cluster size. Indeed, on any finite lattice the ferromagnetic symmetry broken state will not appear and at low enough temperatures one expects Kondo screening of the local moments of the first layer by the second layer light fermions.

It is important to note that the crossover observed in the occupation as a function of cluster size becomes sharper and sharper and seems to extrapolate to fillings lower than $\langle n \rangle_C = 1.58$, as obtained from the coherence temperature. The above allows for an interpretation in

the infinite cluster size limit which is in remarkable agreement with the experimental data of Ref. 18; the QCP is preempted by a first-order transition to a ferromagnetic state. The transition happens when the polarized state becomes more favorable than the Fermi-liquid state stemming from Kondo screening of the local moments of the first layer. This is the case when T_{coh} , i.e. the energy of formation of quasiparticles, becomes smaller than the energy the system gains from a parallel alignment of the f -spins, which is the effective coupling J^* . J^* is composed of two contributions, $J^* = J + J_{\text{eff}}$. The first part is the bare coupling J , while the second is the effective exchange J_{eff} dynamically generated by, e.g., the RKKY interaction. With increasing filling, T_{coh} is suppressed so that the ferromagnetic energy overcomes the coherence scale, and the polarized state becomes the new ground state.

Let us now compare our model calculations to the experimental results of Ref. 18. On the one hand we recover the heavy-fermion state, and the decrease in the coherence scale with increasing filling, with an apparent QCP at a critical filling $\langle n \rangle_C$, which is obtained by extrapolation. On the other hand, we can offer an interpretation for the appearance of an intervening phase with a finite magnetization at a lower filling $\langle n \rangle_I < \langle n \rangle_C$. Since our results support the picture of a first-order transition between competing ground states as a function of μ , the experimental results can be understood as a phase separation, as shown schematically in Fig. 9. This is because in the experiment the filling of ^3He atoms is controlled and not the chemical potential. Thus, the discontinuous behavior with increasing μ in the simulations is mirrored in experiment by the appearance of ferromagnetic islands that are growing in size inside the Fermi liquid of heavy quasiparticles.

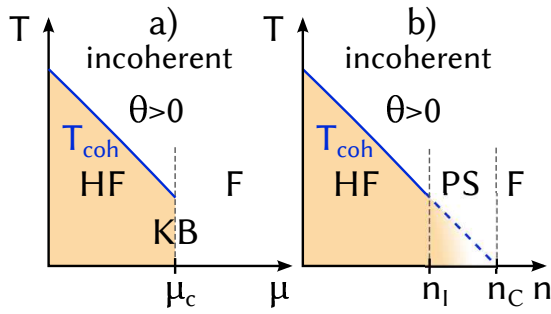


FIG. 9. Schematic phase diagram of the ^3He bilayer as a function of a) chemical potential, and b) total filling. The incoherent phase with a positive (ferromagnetic) Weiss temperature θ crosses over to the coherent heavy fermion state (HF) around the coherence temperature T_{coh} . At the critical chemical potential μ_c , the Kondo effect breaks down (KB) due to the first-order transition to the ferromagnetic state (F). As a function of filling, for $\langle n \rangle > \langle n \rangle_I$ a phase separation (PS) is observed, while extrapolation to a vanishing coherence scale yields the putative QCP at $\langle n \rangle_C$.

The first-order transition brings about an abrupt breakdown of the Kondo effect. In the ferromagnetic

phase we expect the hybridization matrix element at low energies to vanishes. This essentially corresponds to an orbital-selective Mott transition: on orbitals with dominant f -character (i.e. predominantly first layer) we observe a magnet of ferromagnetically coupled, local moments, while on orbitals with dominant c -character (i.e. predominantly second layer) we witness a light Fermi liquid.

ACKNOWLEDGMENTS

We would like to thank J. Saunders for discussions. Funding from the DFG under the Grant No. AS120/6-2 (Forschergruppe FOR 1162) and from the Elite Network of Bavaria is acknowledged. We thank the Jülich Supercomputing Centre for generous allocation of CPU time. The authors gratefully acknowledge the Gauss Centre for Supercomputing e.V. (<http://www.gauss-centre.eu>) for funding this project by providing computing time on the GCS Supercomputer SuperMUC at the Leibniz Supercomputing Centre (LRZ, <http://www.lrz.de>).

-
- * jwerner@physik.uni-wuerzburg.de
- ¹ G. R. Stewart, *Rev. Mod. Phys.* **56**, 755 (1984).
 - ² Z. Fisk, H. R. Ott, T. M. Rice, and J. L. Smith, *Nature* **320**, 124 (1986).
 - ³ M. Sigrist and K. Ueda, *Rev. Mod. Phys.* **63**, 239 (1991).
 - ⁴ P. Gegenwart, Q. Si, and F. Steglich, *Nat. Phys.* **4**, 186 (2008).
 - ⁵ Q. Si, *Phys. Stat. Sol. B* **247**, 476 (2010).
 - ⁶ Q. Si and F. Steglich, *Science* **329**, 1161 (2010).
 - ⁷ P. Coleman and A. H. Nevidomskyy, *J. Low Temp. Phys.* **161**, 182 (2010).
 - ⁸ M. Vojta, *J. Low Temp. Phys.* **161**, 203 (2010).
 - ⁹ Q. Si and S. Paschen, *Phys. Stat. Sol. B* **250**, 425 (2013).
 - ¹⁰ S. Capponi and F. F. Assaad, *Phys. Rev. B* **63**, 155114 (2001).
 - ¹¹ M. Dzero, K. Sun, V. Galitski, and P. Coleman, *Phys. Rev. Lett.* **104**, 106408 (2010).
 - ¹² M. Dzero, K. Sun, P. Coleman, and V. Galitski, *Phys. Rev. B* **85**, 045130 (2012).
 - ¹³ P. Nozières and D. Pines, *The theory of quantum liquids* (Westview Press, 1999).
 - ¹⁴ D. Vollhardt, *Rev. Mod. Phys.* **56**, 99 (1984).
 - ¹⁵ A. Casey, H. Patel, J. Nyéki, B. P. Cowan, and J. Saunders, *J. Low Temp. Phys.* **113**, 293 (1998).
 - ¹⁶ M. Imada, A. Fujimori, and Y. Tokura, *Rev. Mod. Phys.* **70**, 1039 (1998).
 - ¹⁷ M. Dann, J. Nyéki, B. P. Cowan, and J. Saunders, *Phys. Rev. Lett.* **82**, 4030 (1999).
 - ¹⁸ M. Neumann, J. Nyéki, B. Cowan, and J. Saunders, *Science* **317**, 1356 (2007).
 - ¹⁹ D. J. Thouless, *Proc. Phys. Soc.* **86**, 893 (1965).
 - ²⁰ M. Roger, J. H. Hetherington, and J.-M. Delrieu, *Rev. Mod. Phys.* **55**, 1 (1983).
 - ²¹ M. Roger, C. Buerle, H. Godfrin, L. Pricoupenko, and J. Treiner, *J. Low Temp. Phys.* **112**, 451 (1998).
 - ²² P. Werner, A. Comanac, L. de Medici, M. Troyer, and A. J. Millis, *Phys. Rev. Lett.* **97**, 076405 (2006).
 - ²³ K. Haule, *Phys. Rev. B* **75**, 155113 (2007).
 - ²⁴ A. Benlagra and C. Pépin, *Phys. Rev. Lett.* **100**, 176401 (2008).
 - ²⁵ A. Benlagra and C. Pépin, *Phys. Rev. B* **79**, 045112 (2009).
 - ²⁶ A. Rançon-Schweiger, A. Benlagra, and C. Pépin, *Phys. Rev. B* **83**, 073102 (2011).
 - ²⁷ K. S. D. Beach and F. F. Assaad, *arXiv:0905.1127* (2009).
 - ²⁸ K. S. D. Beach and F. F. Assaad, *Phys. Rev. B* **83**, 045103 (2011).
 - ²⁹ G. Kotliar, S. Y. Savrasov, G. Pálsson, and G. Biroli, *Phys. Rev. Lett.* **87**, 186401 (2001).
 - ³⁰ A. Georges, G. Kotliar, W. Krauth, and M. J. Rozenberg, *Rev. Mod. Phys.* **68**, 13 (1996).
 - ³¹ T. Maier, M. Jarrell, T. Pruschke, and M. H. Hettler, *Rev. Mod. Phys.* **77**, 1027 (2005).
 - ³² E. Gull, A. J. Millis, A. I. Lichtenstein, A. N. Rubtsov, M. Troyer, and P. Werner, *Rev. Mod. Phys.* **83**, 349 (2011).
 - ³³ N. Parragh, A. Toschi, K. Held, and G. Sangiovanni, *Phys. Rev. B* **86**, 155158 (2012).
 - ³⁴ K. S. D. Beach, *arXiv:cond-mat/0403055* (2004).